

Properties of Graphite Oxide Powders and Membranes as Revealed by Electron Paramagnetic Resonance Spectroscopy

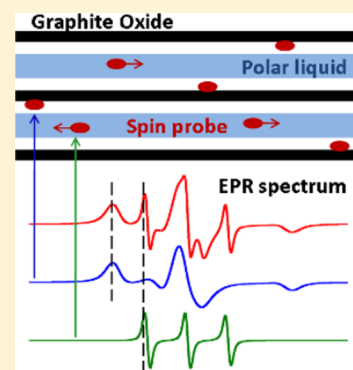
Natalia A. Chumakova,[†] Anastasya T. Rebrikova,[†] Alexandr V. Talyzin,[‡] Nikita A. Paramonov,[†] Andrey Kh. Vorobiev,[†] and Mikhail V. Korobov^{*,†}

[†]Department of Chemistry, Moscow State University, Leninskie Gory 1-3, Moscow 119991, Russia

[‡]Department of Physics, Umeå University, S-90187 Umeå, Sweden

Supporting Information

ABSTRACT: The spin probe technique was used to study graphite oxide (GO) powders swelled in polar liquids (CH₃CN, CH₃OH, and H₂O) and liquid-free GO membranes (GOM). The nitroxide radicals TEMPO (2,2,6,6-tetramethylpiperidine-*N*-oxyl) and TEMPOL (4-hydroxy-2,2,6,6-tetramethylpiperidine-*N*-oxyl) readily penetrated into the interplane space of GO from the solution. Electron paramagnetic resonance (EPR) spectra of these radical probes were sensitive to molecular mobility and orientation ordering within the internal space of GO. The radicals embedded in swelled GO were in two states with different rotational mobilities. The small fraction of radicals located in the interplane space of GO and detected in the broad range of temperatures was in the state of fast rotation, similar to the same radicals dissolved in bulk liquids, thus providing experimental evidence of formation of a liquid-like media within the interplane space of GO. Such mobile media may be responsible for the unusual permeation properties of GOM, which is reported in the literature. Second, less-mobile fraction of radicals was found to be immobilized at the internal surface of GO and was sensitive to phase transformations in the swelled GO structures. The transformations were detected as anomalies at temperature dependences of rotational mobility of radicals. The detected dependence of EPR spectra of probe radicals on orientation of GOM, relative to the direction of magnetic field in the EPR spectrometer, was used for quantitative characterization of orientation alignment of GO planes within the membranes. Such an approach may serve as an elegant method to estimate the relative quality of membranes and other GO-layered structures.



INTRODUCTION

Graphite oxide (GO) is a hydrophilic derivative of graphite,^a which received wide attention recently as a precursor for the preparation of various graphene-based materials.^{2–4} Of particular interest are GO membranes (GOM), which were suggested for filtration and highly selective separation of gaseous and liquid mixtures.^{5–7} GO is a layered structure formed by graphene parallel planes, each of them randomly decorated with oxygen-containing groups (–OH, –O–, COOH–, etc.). GO powders easily swelled in polar liquids, that is, sorption of the liquids into the interplane space, are accompanied by the increase of the interplane distances from ~5 to 7 Å in the dry state up to ~20 Å in the saturated states.^{8,9} The corresponding values of sorption of polar liquids into GO were reported in refs.^{10,11} Swelling and sorption are known to depend on temperature, external pressure, and on the synthesis procedure (Brodie vs Hummers methods, B-GO and H-GO, respectively).^{8,9,12,13} For B-GO, such temperature and pressure dependences take the form of phase transitions in the bulk 3D phases, similar to the incongruent melting transitions in binary systems.^{14,15} However, these transformations, yet, were never examined at the molecular level.

Much attention was attracted to the properties of polar liquids, sorbed into the confined interplane space of GO and

GOM. The mobility of liquids (mostly of water) within the interplane space of GO was examined by several experimental methods; for example, quasi-elastic neutron scattering¹⁶ and neutron diffraction,¹⁷ broadband dielectric spectroscopy,¹⁸ impedance spectroscopy,¹⁹ and so forth. It was demonstrated that sorbed liquids did not experience bulk or confined freezing/melting phase transition.^{11,18} On the basis of this observation, the state of liquids was characterized as “strongly bound to the host molecules”.¹⁸ On the other hand, molecules of water inside GO were reported to possess some rotational freedom.^{16,19} Also, fast permeation of water through GOM²⁰ pointed to certain translational freedom of the H₂O molecules within the interplane space. This translational mobility was attributed to the “hydrophobic regions of pristine graphene capillaries”, where travelling along the interplane space is not hindered by the interaction with oxygen-containing groups of GO.²⁰ Several authors have claimed that the role of hydrophobic unoxidized capillaries was overestimated, and they were not large enough to account for the observed permeation of water.^{21–23} A more comprehensive model of the

Received: July 27, 2018

Revised: September 10, 2018

Published: September 11, 2018



internal structure of hydrated GOM was recently proposed.²⁴ Experimental data²⁰ provoked modeling of movable H₂O structures in the interplane space,^{25–28} and several different low-dimensional ordered forms of structured water were proposed including bi- and trilayers,²⁵ sliding hexagonal ice layers,²⁶ or layers consisting of different coexisting clusters of water.^{27,28} Formation of “square ice” was observed by scanning tunneling microscopy (STM).²⁹ However, the absence of additional reflections in the X-ray diffraction (XRD) spectrum of swelled GO structures points out to the complete disorder of molecules of the sorbed polar liquid in the interplane space.⁹ One may conclude that experimental data on the properties of sorbed liquids inside GO powders and GOM are incomplete and, in part, controversial. Of particular interest are new experimental measurements and methods capable to give a deeper insight into the state of these sorbed polar liquids. Such novel data are of crucial importance, primarily for understanding of liquid permeation through GOM and for rational modeling of filtration and separation processes at GOM.

Recent progress in practical applications of GOM calls for quantitative characterization of their properties and for standardization of the membranes.³⁰ The interplane distance in GOM is one of the key parameters, which can be easily measured by XRD.^{31–33} Another useful characteristic of GOM could be the alignment of the GO layers within the membrane.³² The alignment of layered structures, for example, that of liquid crystals or membranes is frequently characterized by order parameters. The order parameters are values of Legendre functions averaged over all possible orientations.^{34–36}

Analyses of the electron paramagnetic resonance (EPR) spectra of nitroxide radicals (spin probes) embedded in the studied medium is known as a powerful technique, producing detailed information on internal mobility and molecular orientation alignment^{37–44} in different systems. To the best of our knowledge, EPR spectroscopy was never used to examine GO-swelled materials before, though nitroxide radicals were introduced into GO dry films.⁴⁵ In addition, the intrinsic EPR signal of GO was used to characterize GO-based composite materials.^{46,47}

In this study, we apply the spin probe method to examine the B-GO and H-GO powders, saturated with different polar liquids, and liquid-free H-GO membranes. The objectives of this study were to investigate the state and mobility of liquids in the interplane space of GO, detect phase transformations in the swelled GO structures, and monitor the orientation alignment of graphene oxide planes within the dry GOM.

EXPERIMENTAL SECTION

Materials. GO prepared by Hummers' method (H-GO) was purchased from the ACS Material. Samples prepared by Brodie's method (B-GO) were provided by Dr. Szabo, and the synthetic procedure is described elsewhere.⁴⁸ The comparative description of both materials is given in ref 13. The samples were dried to a constant mass in the desiccators with P₂O₅ for 3–5 days.¹¹ The C/O ratio, as measured by X-ray photoelectron spectroscopy after drying, was 2.47 and 2.85, for H-GO and B-GO, respectively. The H-GO membranes were prepared according to the procedure described in ref 23.

Organic solvents utilized (CH₃CN and CH₃OH) were specially redistilled before use. The resulting purity was >99.8%. Milli-Q water was used for measurements.

Introduction of Spin Probes. The structures of spin probe molecules TEMPO (2,2,6,6-tetramethylpiperidin-N-oxyl), TEMPOL (4-hydroxy-2,2,6,6-tetramethylpiperidine-N-oxyl), and ChR (cholestane, 3 β -doxyl-5 α -cholestane) are presented in Figure 1.

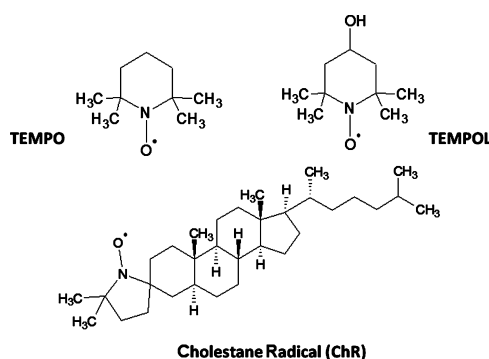


Figure 1. Stable nitroxide radicals used in this study.

To introduce the spin probes into the interlayer space of GO, the radicals were dissolved in the corresponding polar liquid to form solutions with the concentration ~ 1 mmol·L⁻¹, and then 1–2 mg of B-GO/H-GO was mixed with excess of such solutions. The resulting samples were equilibrium heterogeneous mixtures of the swelled GO and of the free solvent as confirmed by equilibrium sorption data.¹¹ Trace amounts of radicals were equilibrated in these two phases. After preparation, some samples were gently dried to remove polar liquid partially or completely. The radicals, therewith, were left within GO. To make the GOM sample for EPR measurements, a free-standing membrane 2–5 μ m thick (see Table 1) and with the diameter of 40 mm was cut into pieces

Table 1. Order Parameters of the H-GO Membranes

membrane (thickness, material)	order parameter	$T = 100$ K ^a	$T = 298$ K ^a
I (~ 5 μ m, H-GO)	P_{20}	0.33	0.25
	P_{40}	0.08	0.04
II (~ 5 μ m, H-GO)	P_{20}	0.35	0.32
	P_{40}	0.07	0.06
III (~ 2 μ m, modified H-GO)	P_{20}	0.34	0.28
	P_{40}	0.14	0.10

^aAccuracy of the numbers in the column is ± 0.01 .

to fit to the EPR tube with the diameter of 4 mm. The probe radicals were introduced into the interplane space of GOM in the same way as introduced into the GO powders (see above). After preparation, the GOM samples were gently dried by heating and pumping in the same manner as for the GO powders and then put into the EPR tube. The mass of the GOM sample in the EPR tube was 1–2 mg.

Some samples were prepared by equilibration of the initially dry radical-containing GO samples with the unsaturated vapors of the polar liquids. By this means, we eliminated the possibility of condensation of bulk polar liquids in the samples and/or filling of the interlamellas' voids in GO powders. The amount of radicals in the samples studied was $\sim 10^{15}$ spin·mg⁻¹. The molar ratio $n_{\text{Radicals}}/n_{\text{GO}}$ was below 2×10^{-5} and in the swelled samples $n_{\text{Radicals}}/(n_{\text{GO}} + n_{\text{Polar liquid}}) < 10^{-5}$. Averaged molecular masses, M_{GO} , of B-GO and H-GO were

estimated as 17.7 and 18.6, respectively. The radicals introduced in such concentrations had little, if any, effect on macroscopic parameters of the samples. (See the [Supporting Information](#) for details of the preparation procedure).

EPR Measurements. EPR spectra were recorded with a Bruker EMX-500 spectrometer over temperatures ranging from 100 to 333 K. A Bruker temperature control unit (accuracy ± 1 K) was applied. The high-sensitive resonator of Bruker ER 4119 HS was used. The time constant in our experiments came to (0.1–0.3) ms. The modulation amplitude was chosen in such a way that no distortion of spectral lines was observed. In our experiments, the value was (0.3–1.0) G. The microwave power used did not cause saturation of EPR signals. The corresponding value in the high-temperature experiments was about 1 mW, whereas in the low-temperature experiments, it lay in the interval (0.3–0.6) mW.

To monitor the orientation distribution of radicals in the GOM, a series of spectra (10–15) were recorded at different orientations of the sample in the magnetic field. The sample was turned around the axis aligned at the surface of the membrane perpendicular to the magnetic field direction. The experiments were performed by means of an automatic goniometer; the accuracy of turning was 0.5° . It was shown that orientation distribution of radicals in the sample kept constant, pending the experiments (during several days).

Experimental EPR Spectra. The EPR spectrum of pristine B-GO is presented in [Figure 2A](#). The EPR signal is an

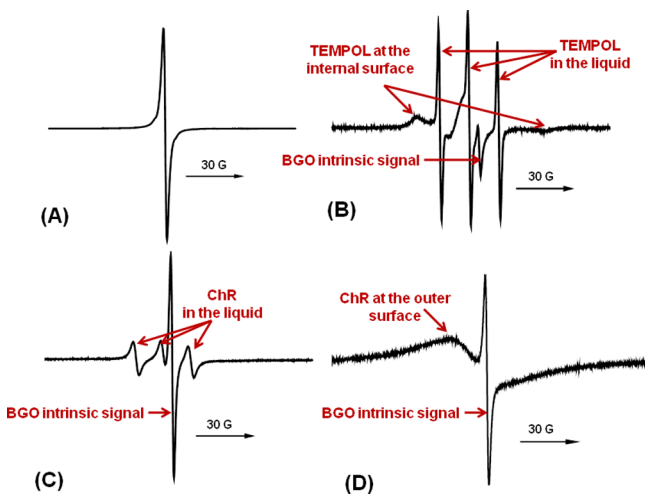


Figure 2. Experimental EPR spectra of different GO samples; (A) intrinsic EPR signal of pristine B-GO; (B) EPR spectrum of the system B-GO-CH₃CN [TEMPOL], $T = 298$ K; (C) EPR spectrum of the system H-GO-CH₃CN [ChR], $T = 235$ K; and (D) EPR spectrum of the system H-GO-CH₃CN [ChR], $T = 100$ K.

unstructured singlet. The H-GO samples have a similar spectrum. In the literature,⁴⁹ this intrinsic EPR signal was attributed to “defects and localized states” and/or to the contribution of the unoxidized graphene-like islands in the sample. [Figure 2B](#) displays the experimental EPR spectrum of the system B-GO-CH₃CN with the radical probe TEMPOL (such a type of systems will be denoted as B-GO-CH₃CN [TEMPOL], etc.). The spectrum is a superposition of the three individual spectra, namely, of the intrinsic spectrum of B-GO and of the spectra of TEMPOL radicals characterized by fast and slow rotational mobility. Fast rotation is typical for the radicals dissolved in the liquid CH₃CN, whereas slow rotation

can be attributed to the radicals sorbed at the internal surface of GO. Similar superposition was observed above the melting point of polar liquid in all of the systems studied, irrespective of the type of GO (H-GO or B-GO), type of the nitroxide radical (TEMPOL or TEMPO), or the polar liquid used. [Figure 2C,D](#) gives the EPR spectra of the system H-GO-CH₃CN [ChR]. The spectra observed with this probe radical differed from those of TEMPOL or TEMPO. The features corresponding to radicals sorbed at the internal surface did not occur in the spectrum. This is an example of a large paramagnetic species which did not penetrate into the internal space of GO. Below the melting temperature of the polar liquids, ChR probes are absorbed at the outer surface of GO ($10\text{--}100\text{ m}^2\text{ g}^{-1}$),⁵⁰ resulting in short distances ($\sim 10^{-9}$ m) between the radicals. The strong magnetic spin exchange and dipole–dipole interactions between paramagnetic species caused the broadened singlet EPR spectrum (see [Figure 2D](#)). Comparison of [Figure 2B–D](#) additionally proves sorption of small radicals TEMPOL and TEMPO at the internal surface of GO.

Change in the shape of the spectral line with the temperature indicates a change in the ratio of the numbers of paramagnetic species in the liquid and at the surface. When cooling the sample, the number of radicals at the surface increases. At $T = 100$ K, already all probe radicals are immobilized at the internal surface of GO. No probe radicals are left within the frozen liquid. The shape of the EPR spectrum recorded in such conditions is typical for nitroxide radicals in the absence of rotational mobility (in the rigid limit) (see [Figure 3A](#)).

EPR Spectra Simulations. Simulations of rigid-limit EPR spectra of spin probes in the systems GO–polar liquid [nitroxide radical] (see [Figure 3](#)) were performed using the explicit formulas within the perturbation theory of the second

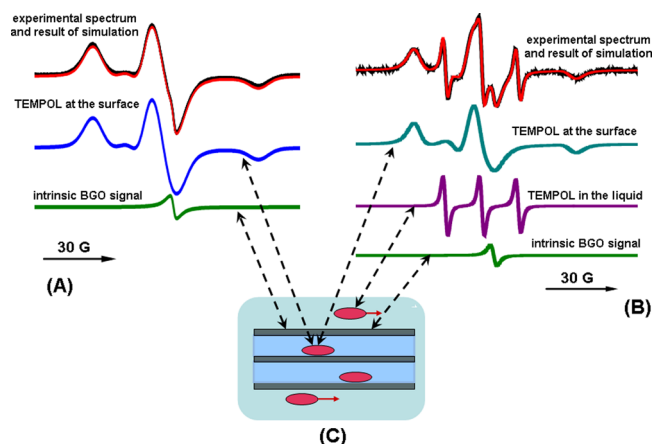


Figure 3. Experimental and simulated EPR spectra in the system B-GO-CH₃CN [TEMPOL]. Black lines represent experimental EPR spectra of the system; colored lines represent results of simulations of the total spectra and of the contributions from different components. (A) $T = 100$ K, rigid limit; (B) $T = 235$ K, above the melting point of CH₃CN ($T_{\text{melt}} = 229$ K). Both in (A,B), experimental and simulated spectra practically coincide; and (C) schematic illustration of the B-GO-CH₃CN [TEMPOL] sample. B-GO planes (black), external (mid-blue), and sorbed (deep blue) CH₃CN, TEMPOL radicals (red circles), sorbed at the internal surface of B-GO and dissolved in external CH₃CN are shown. Double arrows connect parts of the sample with the corresponding peaks in the EPR spectra.

order.⁵¹ The detailed description of the method is presented in ref 42. Each rigid limit spectrum was considered as a sum of two signals—signal of the sorbed nitroxide radicals with no rotational mobility and the intrinsic signal of the carbon material. In Figure 3A, the experimental spectrum of the system is compared with the simulated spectra of both components and their sum. The parameters of both component signals were varied in the course of simulation. The complete list of magnetic parameters of TEMPO and TEMPOL in the systems studied is given in the Supporting Information.

The EPR spectra at temperatures above the melting points of the liquids were simulated, taking into account rotational diffusion of the radicals. The simulation was performed using the method based on solving of the stochastic Liouville equation.^{37–39} In this case, each spectrum was considered as a sum of the three signals: the signal of nitroxide radicals sorbed at the internal surface of GO, the signal of nitroxide radicals in the free liquid, and the intrinsic GO signal (see Figure 3B). As a result, the rotational diffusion coefficients of the nitroxide paramagnetic species, dissolved in the liquid and sorbed at the GO surface, and the ratio of the numbers of these two types of radicals, N_{dis} and N_{sorb} , respectively, were found. The variation of parameters was performed using the NLSOL procedure.⁵²

EPR Spectra Simulations in the Experiments with Variable Orientation of the Sample in the Magnetic Field. To determine the radical's orientation distribution, the simultaneous simulation of the spectra recorded at different orientations of the sample in the magnetic field was performed. The spectra recorded at 100 K, in the absence of the rotational mobility of paramagnetic species, were simulated according to the method described in ref 42. The orientation distribution function of the radicals was presented as a series of spherical harmonics

$$\rho(\beta, \gamma) = \sum_{j=0}^{\infty} \left[\frac{1}{2} a_{j0} P_j(\cos \beta) + \sum_{k=1}^j P_j^k(\cos \beta) \right. \\ \left. (a_{jk} \cos(k\gamma) + b_{jk} \sin(k\gamma)) \right] \quad (1)$$

where $P_j(\cos \beta)$ are Legendre polynomials, $P_j^k(\cos \beta)$ are associated Legendre functions, and angles β and γ characterize the orientation of the sample symmetry axis (surface normal vector) in the magnetic reference frame of the nitroxide radicals. The coefficients a_{j0} , a_{jk} , b_{jk} in eq 1 are variable parameters. Because of the orthorhombic symmetry of magnetic characteristics of the nitroxide radicals, only coefficients a_{jk} with even j and k can be nonzero. These nonzero coefficients were found as a result of spectra simulation. From them, the order parameters $P_{20} = a_{20}/5$ and $P_{40} = a_{40}/9$ (see Table 1) were calculated. The parameters of higher ranks were not reflected in the EPR spectra. At ambient temperature, the local orientation of TEMPOL radicals at the internal surface of H-GOM was described by the mean field potential approach,^{37–39} and the orientation distribution of the local directors was presented as a series (eq 1). The computer program described in ref 39 was modified to take into account the orientation distribution function. The rotational diffusion coefficients were varied together with the coefficients in eq 1 in the course of simulation. The spin-Hamiltonian parameters (magnetic parameters) of radicals

were taken as for the corresponding systems with the H-GO powders (see the Supporting Information for details).

RESULTS AND DISCUSSION

Phase Transformation in the Binary Systems B-GO–CH₃CN and B-GO–CH₃OH. Experiments performed here revealed that the lowest and the highest field components of the EPR spectrum change their positions and intensity with the change of temperature (see Figure 4). These components

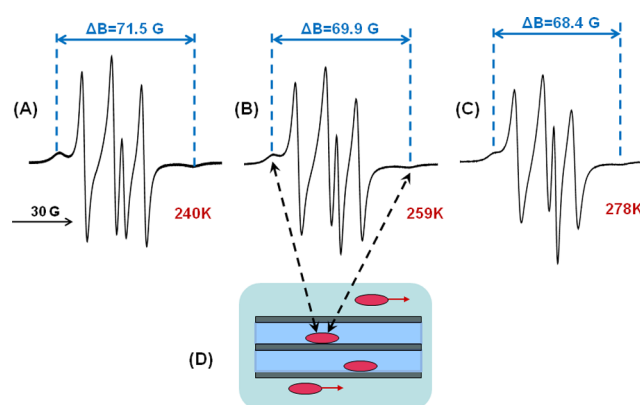


Figure 4. Experimental EPR spectra of the system H-GO–CH₃CN [TEMPOL] recorded at different temperatures. Blue double arrows show the distance, ΔB , between the lowest and the highest components of the spectra. (A) $T = 240$ K; (B) $T = 259$ K; (C) $T = 278$ K; and (D) schematic illustration of the H-GO–CH₃CN [TEMPOL] sample. Dashed double arrows connect the TEMPOL radical (red circle), sorbed at the internal surfaces of H-GO with the corresponding peaks in the EPR spectra.

belong to the signal of the radicals sorbed at the internal GO surface. The distance between them, ΔB , is known to correlate with the rotational mobility of the paramagnetic species.⁵³ Decrease in the distance in the experimental spectra reflects an increase in the rotational mobility. Figure 4 presents the spectra of the system H-GO–CH₃CN [TEMPOL], recorded at 240–278 K.

Figure 5A,B shows the experimental temperature dependencies of ΔB for TEMPOL in B-GO–CH₃CN and in H-GO–CH₃CN along with the temperature dependencies of the corresponding rotation diffusion coefficients, D , estimated by simulation of EPR spectra. In the case of H-GO, the values of ΔB decrease and the values of D increase monotonously with temperature increase. This indicates the increase of rotation mobility of the sorbed radicals at higher temperatures. In the case of B-GO, the dependences of both ΔB and D on temperature are nonmonotonous, and the sharp anomaly in the radical's mobility is observed at $T \approx 267$ – 300 K. Similar nonmonotonous temperature dependencies of ΔB and D were detected for radicals TEMPO in the system B-GO–CH₃OH. The effects were reversible on cooling. Absolute values of diffusion coefficients (5.3×10^6 to 2.4×10^7 s⁻¹) point clearly toward restricted motion of the sorbed TEMPOL and TEMPO and are close, for example, to those of nitroxide radicals adsorbed into X zeolites.⁵⁴

Earlier incongruent melting of the swelled structures was detected in B-GO–CH₃CN and B-GO–CH₃OH systems using DSC and temperature-programmed XRD.^{14,15} In the system B-GO–CH₃CN, the reversible transition of the low temperature phase into the high temperature phase with the

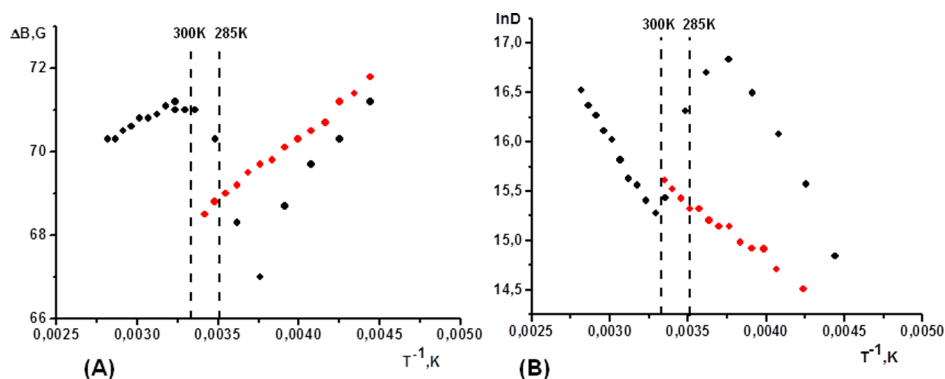


Figure 5. Temperature dependencies of ΔB and of rotational diffusion coefficients, D , of TEMPOL radicals in the systems H-GO-CH₃CN and B-GO-CH₃CN. Measurements were taken on heating the samples. Vertical dashed lines mark the temperature interval, where phase transformation in B-GO-CH₃CN was detected by differential scanning calorimetry (DSC) and XRD.¹⁴ (A) ΔB vs T^{-1} , TEMPOL in H-GO-CH₃CN (red circles), TEMPOL in B-GO-CH₃CN (black circles), (B) $\ln D$ vs T^{-1} , TEMPOL in H-GO-CH₃CN (red circles), TEMPOL in B-GO-CH₃CN (black circles).

release of part of the sorbed liquid at $T = 285\text{--}300$ K was found on heating. The low temperature phase was interpreted as the swelled structure with two layers of CH₃CN inserted between GO planes [$d(001) = 12$ Å], whereas the high temperature phase is intercalated with only one CH₃CN layer [$d(001) = 9$ Å].¹⁵ The smaller interlayer distance in the high-temperature phase hinders the rotational mobility of the radicals, sorbed at the surface. This explains the sharp decrease of the rotational mobility observed in Figure 5 for TEMPOL in B-GO-CH₃CN. When phase transformation is completed ($T = 300$ K), the increase of rotational mobility with temperature continues. In contrast, the H-GO-CH₃CN system shows slow, monotonous increase of the rotational mobility of the radicals with temperature (see Figure 5, red circles). Two apparently contrary reasons seem to be responsible for such behavior: (a) increase of temperature and (b) monotonous decrease of the interplane distance in the swelled H-GO with the increase of temperature. No phase transformation was detected in the H-GO-CH₃CN system by DSC.¹⁵

Figure 5 clearly demonstrates that phase transformation from the low to the high-temperature B-GO-CH₃CN swelled structure occurs over a wide temperature interval rather than at a certain temperature point. This is because of the inherently nonuniform composition of the swelled B-GO powders. Strictly speaking, the observed transformation is not a first-order phase transition in the thermodynamic sense, though the difference in behavior between the B-GO-CH₃CN swelled structure (phase transformation) and H-GO-CH₃CN (no phase transformation; continuous change) is obvious from EPR spectra. EPR measurements are more sensitive compared to XRD and DSC, and they detect the beginning of phase transformation at much lower temperatures. Activation energies of rotation diffusion of radicals may be additionally derived from Figure 5B. Thus, EPR gives deeper insight into the physical nature of the phase transformations in the swelled GO structures rather than simply confirming their detection by routine methods.

“Fast Components” in the EPR Spectra and Liquid-Like Fraction in the Interplane Space. Figure 6 gives EPR spectra of the systems H-GO-CH₃CN [TEMPO] and B-GO-CH₃CN [TEMPO] at temperatures 230 and 220 K (above and below the acetonitrile melting point, $T = 229$ K), respectively. Above the melting point, the strong signal of narrow components, characteristic of the fast rotating radicals

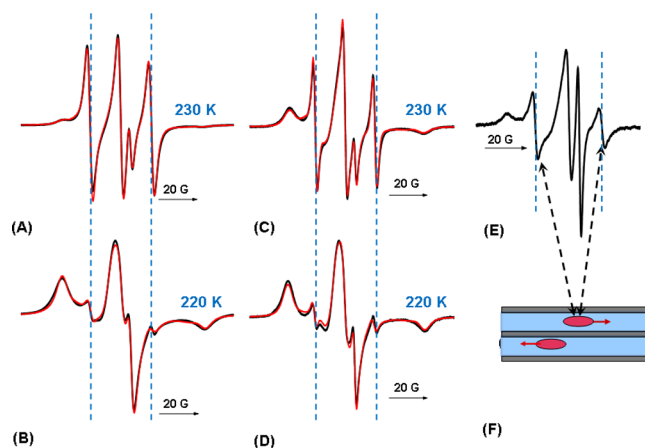


Figure 6. EPR spectra of the systems H-GO-CH₃CN [TEMPO] and B-GO-CH₃CN [TEMPO] taken above (230 K) and below (220 K) the melting point of CH₃CN ($T_{\text{melt}} = 229$ K). (A,B) H-GO-CH₃CN [TEMPO]; (C,D) B-GO-CH₃CN [TEMPO]; (E) EPR spectrum in the system B-GO-CH₃CN [TEMPO] ($T = 280$ K) after removing the free acetonitrile from the system. Black lines are experimental spectra and red lines are the result of simulation. Fast components are marked with dashed lines; and (F) schematic illustration of the sample (E). Only the radicals responsible for the “fast components” in the EPR spectra are shown. Double arrows connect the radical with the corresponding peaks in the EPR spectrum.

in the free liquid CH₃CN, is readily seen in the spectra. Surprisingly, a small portion of this signal is still visible in the spectra recorded after acetonitrile freezing (see Figure 6B,D). This fraction of fast radicals constituted about 2% of the total amount of spins in the system. The fraction was not detected in the blank experiment when the solution of TEMPO in pure liquid CH₃CN was frozen. The same fast components were observed in the spectra of TEMPO in the unsaturated sample of the B-GO-CH₃CN system recorded at room temperature (see Figure 6E). Free acetonitrile was gently removed from this sample, and the residual amount of CH₃CN constituted less than 70% of the value of the saturated sorption.¹¹ The absence of the accidental free liquid acetonitrile in the sample was checked by DSC.

Analogous “fast components” of the spectra were observed for radicals TEMPO in the system H-GO-H₂O (see Figure 7) below the melting point of water. In this case, the fraction of

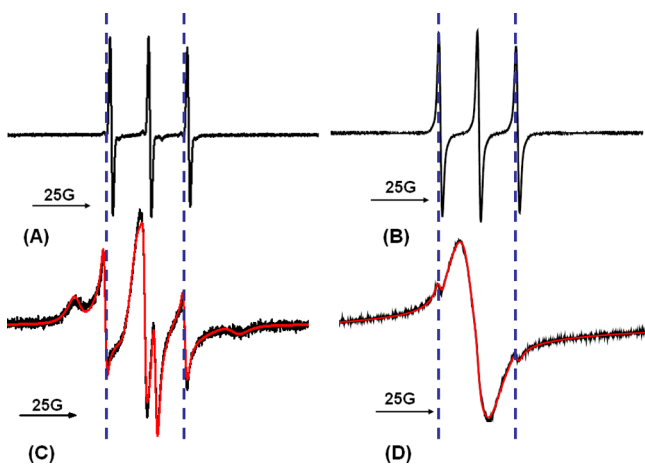


Figure 7. EPR spectra of the systems H-GO–H₂O [TEMPO] and H₂O [TEMPO] (blank experiment) recorded above and below the melting point of H₂O. Black lines are experimental spectra and red lines are the result of simulation. Peaks of fast rotating fraction are marked with dashed lines. (A,C) H-GO–H₂O [TEMPO] above and below $T = 273$ K, respectively; (B,D) H₂O [TEMPO] (blank experiment without H-GO) above and below $T = 273$ K, respectively.

fast rotating radicals comes to 6%, whereas in the blank experiment, this fraction makes up $\sim 0.3\%$ of the total amount of spins. Hence, the appearance of the fast-rotating radicals in this system is also because of the presence of GO. In both H-GO/B-GO–CH₃CN and H-GO–H₂O systems, the fraction of fast-rotating radicals monotonously decreases with temperature and disappears at temperatures 45 and 25° below the melting temperatures of CH₃CN and H₂O, respectively.

Fast components were also detected in the initially liquid-free B-GO [TEMPO] samples equilibrated with the unsaturated vapors of polar liquids (CH₃OH, H₂O, and CH₃CN) at $T = 303$ – 333 K (see the Supporting Information for detailed description of the experimental setup). In this case, the degree of vapor pressure saturation of polar liquids was a variable parameter, and fast components were visible at pressures starting from $\sim 50\%$ of the saturated value at the corresponding temperature (see Figure 8). For CH₃CN, the rotating fraction was observed even at 24% of the saturated vapor pressure ($T =$

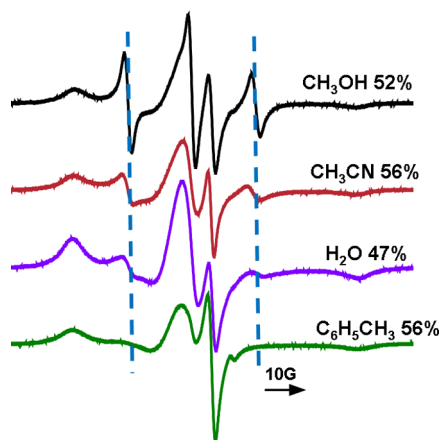


Figure 8. EPR spectra of B-GO [TEMPO] equilibrated with the unsaturated vapors of polar liquids and toluene at $T = 311$ K; numbers in percent are relative saturation of vapors; dashed lines mark the peaks of fast-rotating fraction of radicals TEMPO.

333 K). Such low pressures prevent formation of bulk liquid phases in the samples. For nonpolar toluene, which is not sorbed into the interplane space of GO, the fast components were not detected in the EPR spectrum (see Figure 8). In the experiment with the H-GO membrane, the H-GOM [TEMPO] sample was equilibrated with CH₃CN vapor, and the rotating fraction was detected at 55% of the saturated vapor pressure.

The rotating fraction of TEMPO in Figures 6–8 is located either in the interplane space or in the interlamella voids of GO along with the molecules of corresponding polar liquids. Buchsteiner et al.¹⁶ claimed that H₂O in the interlamella space was detected by quasi-elastic neutron scattering in the B-GO–H₂O system at relative humidity (RH) above 75%. This corresponds to the characteristic size of the interlamella space, $d \geq 3.4$ nm. Below this level, H₂O was detected only in the interplane space of GO. In our experiments, the traces of rotating fraction were found beginning from 47% RH for H₂O (see Figure 8). For other polar liquids, the rotating fraction was detected at similar or even lower degrees of relative saturation (see Figure 8). Such low saturations prevent condensation into the interlamella voids with the characteristic size above 2 nm (see the Supporting Information for discussion).

On the basis of the results obtained, we claim that a freely rotating fraction of TEMPO is located within the interplane space of GO and GOM. The rotational motion appeared only in the swelled samples and is associated with the presence of molecules of polar liquids in the same space. The rotational motion of TEMPO in such an environment is similar to the one in the bulk liquid phase and is kept below the melting point of the bulk liquid (see Figures 6 and 7). Such motion was also evident in the unsaturated GO samples at temperatures near ambient in the absence of bulk liquid (see Figures 6E and 8).

The rotational freedom of radicals in turn points to the formation of some liquid-like media with the corresponding rotational and translational freedom in the narrow interplane space of GO in the systems “H-GO, B-GO–polar liquid”. Such liquid-like media is undetectable for XRD.⁸ The above-mentioned fast-rotating radicals are located within this media. The interplane distance in H-GO and B-GO samples discussed is ~ 9 Å at ambient temperature. In hydrophilic areas, part of this distance is taken by oxygen-containing groups at the GO planes (~ 1.5 Å near each plane). This does not leave enough room for fast rotation of TEMPO whose effective size is ~ 6.6 Å. It may be assumed that liquid-like media with the fast-rotating radicals mostly occupies “hydrophobic capillaries”²⁰ within B-GO and H-GO with no oxygen-containing groups at the surface there.

Nair et al.,²⁰ who first observed rapid permeation of H₂O through GOM, have mentioned the classical liquid diffusion as a preferable mechanism of this process. Such a mechanism calls for “highly mobile...monolayer water”²⁰ inside the interplane space. It worth noting that considerable permeation through GOM started to occur at $\text{RH} \approx 50\%$,²⁰ and rotating fraction of radicals appeared in our experiment almost at the same RH (see Figure 8). Our data experimentally confirm formation of the mobile media inside GO, though not exceptionally for water. The same media was detected at least for two other polar liquids, CH₃CN and CH₃OH, as well.

Orientation Alignment of GOM. The experimental data obtained (see Figure 9) demonstrated strong dependence of the EPR spectra of the H-GO membranes (H-GOM) with the

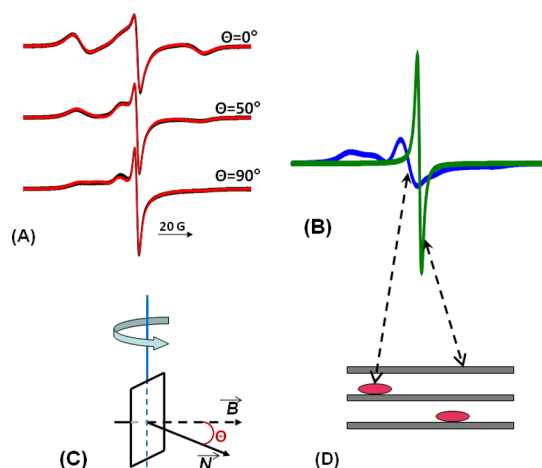


Figure 9. Angular dependences of the EPR spectra of the system H-GOM [TEMPOL]. (A) $T = 100$ K. Black lines are experimental spectra, red lines—result of simulation. Numbers, for example, 90° , are angles, θ , between the direction of vector N and the magnetic field direction, B ; (B) contributions of TEMPOL radicals (blue line) and of the intrinsic signal of H-GOM (green line) into the experimental spectrum, $T = 100$ K, $\theta = 90^\circ$; (C) rotation of the sample relative to the direction of the magnetic field, B (see the text for details); (D) schematic illustration of the H-GOM [TEMPOL] sample. Double arrows connect parts of the sample with the corresponding peaks in the EPR spectra.

introduced radical TEMPOL, [this system will be denoted as H-GOM (TEMPOL)], on the orientation of the sample relative to the magnetic field direction in the EPR spectrometer. H-GOMs were liquid-free, and the spectra were a superposition of the intrinsic spectrum of H-GO and of the spectrum of TEMPOL radicals sorbed at the internal surface of H-GOM. Figure 9A presents angular dependences recorded at $T = 100$ K (in rigid limit) and the results of simulations of the spectra. The similar results were obtained at $T = 298$ K (see the Supporting Information for details). Comparison of Figure 9A,B demonstrates that a major part of the angular dependence of the spectrum was associated with the contribution from sorbed TEMPOL radicals. In the present study, we were focused on this contribution, though the intrinsic EPR spectrum of H-GOM also slightly depended on the orientation.

In all membranes studied and at both temperatures, the orientation distribution of sorbed radicals was found to be uniaxial. The symmetry axis is the normal vector, N , to the membrane's surface. In all cases, simulation of the spectra gave the order parameters P_{20} and P_{40} , and the values P_{22} , P_{42} , and P_{44} were found to be zero. These parameters characterize the orientation of radicals relative to the vector N . Adding the higher rank parameters did not improve the description of the spectra.

The order parameters, calculated from the angular dependences of the experimental EPR spectra for the three different H-GO membranes, are presented in Table 1. They are determined by two physical factors, for example, P_{20} is a product

$$P_{20} = P_{20}(\text{GOM}) \times P_{20}(\text{TEMPOL})$$

where $P_{20}(\text{GOM})$ and $P_{20}(\text{TEMPOL})$ are the order parameters determined by the averaged alignment of the GO planes within the membrane and by the averaged orientation of

radical TEMPOL relative to H-GO planes, respectively. The latter factor makes the order parameters rather low, though it is not changed from membrane to membrane. In the case of ideally parallel planes and of identical orientation of probe radicals relative to the H-GO plane, the order parameter P_{20} , $P_{20}(\text{GOM})$, and $P_{20}(\text{TEMPOL})$ will be equal to unity. The same relations are valid for P_{40} . The values of P_{20} and P_{40} obtained for a series of membranes with one and the same radical can be considered as relative quantitative characteristics of parallelism of GO planes in the GOM. The membranes I and II were prepared by the same method²³ and had similar thickness ($\sim 5 \mu\text{m}$). The membrane III was thinner ($\sim 2 \mu\text{m}$) and was made out of H-GO prepared by the modified Hummers method.⁵⁵ It is seen from the table that order parameters in all of the membranes studied are close. Also, the extent of the orientation alignment is somewhat higher in cooled samples, where the rotational mobility is hindered. This makes measurements at the rigid limit ($T = 100$ K) more informative.

Figure 10A–C demonstrates the orientation distribution functions of spin probes in the membranes which show

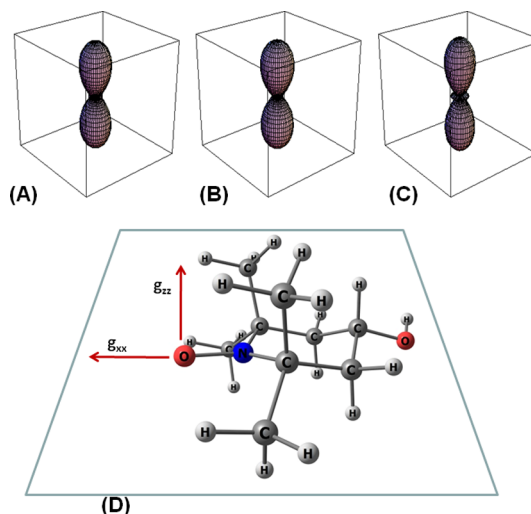


Figure 10. Orientation distribution functions of spin probes in H-GOM, $T = 100$ K (rigid limit). (A) Membrane I; (B) membrane II; (C) membrane III, narrow "belt" in the center corresponds to disordered radicals randomly distributed in space; and (D) orientation of TEMPOL radical relative to the GO plane.

orientation of g_{zz} axes of the nitroxide radicals relative to the membrane normal vector N . The functions unambiguously indicate the preferential orientation of the radicals with respect to the membrane surface (see Figure 10D). The figure demonstrates that the ring plane of the TEMPOL radical is approximately parallel to the GO plane. The molecular g_{zz} axis is preferentially directed along the vector N , but molecular g_{xx} and g_{yy} axes are randomly oriented along the GO plane. A similar orientation of nitroxide radicals at the GO surface was observed earlier by the authors.⁴⁵ It is most likely that such an orientation is caused by the interaction of OH and NO groups of the radicals with the oxygen-containing groups at the GO surface.

Figure 10 shows that orientation functions of TEMPOL in membranes I and II are practically the same, whereas in membrane III, there is some amount of disordered para-

magnetic species. Apparently, these radicals are located in defective areas of the membrane.

Overall, it can be concluded that EPR spectroscopy is a perspective method to study the orientation alignment of the planes in the GOM. It can be used for determination of the extent of alignment and for estimation of the number of defects within the membrane. Both characteristics can serve to assess the quality of a membrane. The closest task would be selection of a series of radicals which are most uniformly oriented relative to the planes and are sensitive to own the orientation alignment of the planes within GO.

CONCLUSIONS

In the present study, the EPR in combination with the spin probes technique was used for the first time to examine the GO powders swelled in polar liquids and the liquid-free (dried) GOM. The method demonstrated unique capabilities in revealing several properties of the systems “GO–polar liquid”. In a number of independent experiments, freely rotating radicals were detected, particularly in the interplane space of the swelled H-GO and B-GO powders and H-GO membranes in the broad range of temperatures, from ambient temperature down to the temperatures well below the melting points of the polar liquids. The rotating mobility of these radicals was similar to the one in the bulk liquids and points to the formation of liquid-like and rotationally and translationally mobile media in the narrow space between the graphene oxide planes. The effect was observed for water, acetonitrile, and methanol. It was additionally proved that the corresponding EPR signal did not originate from the interlamella voids of the samples. Taking into account the effective size of rotating radicals, one may conclude that these radicals, along with the liquid-like media, are located in the hydrophobic channels inside GO, that is, in the areas with no oxygen-containing groups at the surface. Only in such areas, there will be enough space for free rotation. Formation of “liquid- or ice-like” mobile layers, suggested previously in a series of theoretical models, was clearly evidenced now by EPR measurements. Previously, no other method provided such a set of experimental information on the state of sorbed liquids in the GO-swelled structures. A comparative study of the mobile fractions of different polar liquids in the GO structures is on demand.

Another part of the EPR spectrum, corresponding to the rotationally restricted radicals immobilized at the internal surface, provided detailed information on the incongruent melting in the swelled B-GO structures. The mobility of the sorbed radicals was found to change abruptly at temperatures of such phase transformations. EPR was proved to be more sensitive to these phenomena compared to the conventional methods (XRD and DSC). One may assume that because of its sensitivity, EPR with spin probing may be used to search and to study phase transformations in a variety of the graphene oxide structures, that is, in membranes, thin films and papers, where XRD and calorimetry are hardly applicable.

We also observed the pronounced dependence of the EPR spectra of probe radicals in the GOM over the orientation of the sample in the magnetic field of the EPR spectrometer. Less pronounced but measurable was the orientation dependence of the intrinsic EPR spectra of GOM. Such effects provide the basis for the quantitative description of orientation ordering within the GOMs. Analysis of EPR spectra readily gives order parameters characterizing the staking order of the graphene

oxide planes in the GOMs. In addition, the amount of defects in the membrane can be quantitatively estimated from the measured quantity of disordered radicals. EPR spectra along with XRD may serve as a paramount tool for characterization and standardization of the GOMs. This is of special interest for various practical applications. EPR data could be useful in comparing and improving the preparation methods and in gaining performance of the synthesized GOM.

ASSOCIATED CONTENT

Supporting Information

The Supporting Information is available free of charge on the ACS Publications website at DOI: 10.1021/acs.jpcc.8b07221.

Preliminary treatment of the samples for EPR measurements, spin-Hamiltonian parameters of radicals TEMPO and TEMPOL in the systems GO–polar liquid and in organic liquids, experimental setup for EPR measurements with the GO samples in equilibrium with the unsaturated vapors of polar liquids, and angular dependences of EPR spectra of H-GOM [TEMPOL] at 100 and 298 K (PDF)

AUTHOR INFORMATION

Corresponding Author

*E-mail: mkorobov49@gmail.com.

ORCID

Alexandr V. Talyzin: 0000-0002-3320-8487

Andrey Kh. Vorobiev: 0000-0002-6701-0524

Mikhail V. Korobov: 0000-0002-0099-9008

Notes

The authors declare no competing financial interest.

ACKNOWLEDGMENTS

A.T.R. acknowledges financial support from the Russian Foundation for Basic Research (RFBR) grant no 18-33-00439.

ADDITIONAL NOTE

“We use the term “Graphite oxide” rather than “Graphene oxide” in accordance with the nomenclature recommended in ref 1.

REFERENCES

- (1) Bianco, A.; Cheng, H.-M.; Enoki, T.; Gogotsi, Y.; Hurt, R. H.; Koratkar, N.; Kyotani, T.; Monthieux, M.; Park, C. R.; Tascon, J. M. D.; Zhang, J. All in the graphene family - A recommended nomenclature for two-dimensional carbon materials. *Carbon* **2013**, *65*, 1–6.
- (2) Chen, D.; Feng, H.; Li, J. Graphene Oxide: Preparation, Functionalization, and Electrochemical Applications. *Chem. Rev.* **2012**, *112*, 6027–6053.
- (3) Singh, R. K.; Kumar, R.; Singh, D. P. Graphene Oxide: Strategies for Synthesis, Reduction and Frontier Applications. *RSC Adv.* **2016**, *6*, 64993–65011.
- (4) Georgakilas, V.; Tiwari, J. N.; Kemp, K. C.; Perman, J. A.; Bourlino, A. B.; Kim, K. S.; Zboril, R. Noncovalent Functionalization of Graphene and Graphene Oxide for Energy Materials, Biosensing, Catalytic, and Biomedical Applications. *Chem. Rev.* **2016**, *116*, 5464–5519.
- (5) Sun, P.; Wang, K.; Zhu, H. Recent Developments in Graphene-Based Membranes: Structure, Mass-Transport Mechanism and Potential Applications. *Adv. Mater.* **2016**, *28*, 2287–2310.
- (6) Liu, G.; Jin, W.; Xu, N. Graphene-Based Membranes. *Chem. Soc. Rev.* **2015**, *44*, 5016–5030.

- (7) Ma, J.; Ping, D.; Dong, X. Recent Developments of Graphene Oxide-Based Membranes: A Review. *Membranes* **2017**, *7*, 52–79.
- (8) You, S.; Sundqvist, B.; Talyzin, A. V. Enormous Lattice Expansion of Hummers Graphite Oxide in Alcohols at Low Temperatures. *ACS Nano* **2013**, *7*, 1395–1399.
- (9) Talyzin, A. V.; Solozhenko, V. L.; Kurakevych, O. O.; Szabó, T.; Dékány, I.; Kurnosov, A.; Dmitriev, V. Colossal Pressure-Induced Lattice Expansion of Graphite Oxide in the Presence of Water. *Angew. Chem., Int. Ed.* **2008**, *47*, 8268–8271.
- (10) Barroso-Bujans, F.; Cervený, S.; Alegría, A.; Colmenero, J. Sorption and Desorption Behavior of Water and Organic Solvents from Graphite Oxide. *Carbon* **2010**, *48*, 3277–3286.
- (11) Korobov, M. V.; Talyzin, A. V.; Rebrikova, A. T.; Shilayeva, E. A.; Avramenko, N. V.; Gagarin, A. N.; Ferapontov, N. B. Sorption of Polar Organic Solvents and Water by Graphite Oxide: Thermodynamic Approach. *Carbon* **2016**, *102*, 297–303.
- (12) Talyzin, A. V.; Luzan, S. M.; Szabó, T.; Chernyshev, D.; Dmitriev, V. Temperature dependent structural breathing of hydrated graphite oxide in H₂O. *Carbon* **2011**, *49*, 1894–1899.
- (13) You, S.; Luzan, S. M.; Szabó, T.; Talyzin, A. V. Effect of Synthesis Method on Solvation and Exfoliation of Graphite Oxide. *Carbon* **2013**, *52*, 171–180.
- (14) You, S.; Luzan, S.; Yu, J.; Sundqvist, B.; Talyzin, A. V. Phase Transitions in Graphite Oxide Solvates at Temperatures Near Ambient. *J. Phys. Chem. Lett.* **2012**, *3*, 812–817.
- (15) Talyzin, A. V.; Klechikov, A.; Korobov, M.; Rebrikova, A. T.; Avramenko, N. V.; Gholami, M. F.; Severin, N.; Rabe, J. P. Delamination of Graphite Oxide in a Liquid upon Cooling. *Nanoscale* **2015**, *7*, 12625–12630.
- (16) Buchsteiner, A.; Lorf, A.; Pieper, J. Water Dynamics in Graphite Oxide Investigated with Neutron Scattering. *J. Phys. Chem. B* **2006**, *110*, 22328–22338.
- (17) Cabrillo, C.; Barroso-Bujans, F.; Fernandez-Perea, R.; Fernandez-Alonso, F.; Bowron, D.; Bermejo, F. J. Absorbate-Induced Ordering and Bilayer Formation in Propanol-Graphite-Oxide Intercalates. *Carbon* **2016**, *100*, 546–555.
- (18) Cervený, S.; Barroso-Bujans, F.; Alegría, A.; Colmenero, J. Dynamics of Water Intercalated in Graphite Oxide. *J. Phys. Chem. C* **2010**, *114*, 2604–2612.
- (19) Yu, J.; Gu, M.; Bian, C.; Xu, X.; Tang, T. B. An Impedance Spectroscopy Study of the Rotation and Reorientation of Water Molecules in Hydrated Graphite Oxide. *Carbon* **2013**, *61*, 367–372.
- (20) Nair, R. R.; Wu, H. A.; Jayaram, P. N.; Grigorieva, I. V.; Geim, A. K. Unimpeded Permeation of Water through Helium-Leak-Tight Graphene-Based Membranes. *Science* **2012**, *335*, 442–444.
- (21) Erickson, K.; Ermi, R.; Lee, Z.; Alem, N.; Gannett, W.; Zettl, A. Determination of the Local Chemical Structure of Graphene Oxide and Reduced Graphene Oxide. *Adv. Mater.* **2010**, *22*, 4467–4472.
- (22) Pacilé, D.; Meyer, J. C.; Fraile Rodríguez, A.; Papagno, M.; Gómez-Navarro, C.; Sundaram, R. S.; Burghard, M.; Kern, K.; Carbone, C.; Kaiser, U. Electronic Properties and Atomic Structure of Graphene Oxide Membranes. *Carbon* **2011**, *49*, 966–972.
- (23) Klechikov, A.; Yu, J.; Thomas, D.; Sharifi, T.; Talyzin, A. V. Structure of Graphene Oxide Membranes in Solvents and Solutions. *Nanoscale* **2015**, *7*, 15374–15384.
- (24) Williams, C. D.; Carbone, P.; Siperstein, F. R. Computational characterisation of dried and hydrated graphene oxide membranes. *Nanoscale* **2018**, *10*, 1946–1956.
- (25) Wei, N.; Peng, X.; Xu, Z. Breakdown of Fast Water Transport in Graphene Oxides. *Phys. Rev. E: Stat., Nonlinear, Soft Matter Phys.* **2014**, *89*, 012113.
- (26) Boukhalov, D. W.; Katsnelson, M. I.; Son, Y.-W. Origin of Anomalous Water Permeation through Graphene Oxide Membrane. *Nano Lett.* **2013**, *13*, 3930–3935.
- (27) Willcox, J. A. L.; Kim, H. J. Molecular Dynamics Study of Water Flow across Multiple Layers of Pristine, Oxidized, and Mixed Regions of Graphene Oxide. *ACS Nano* **2017**, *11*, 2187–2193.
- (28) Willcox, J. A. L.; Kim, H. J. Molecular Dynamics Study of Water Flow Across Multiple Layers of Pristine, Oxidized, and Mixed Regions of Graphene Oxide: Effect of Graphene Oxide Layer-to-Layer Distance. *J. Phys. Chem. C* **2017**, *121*, 23659–23668.
- (29) Algara-Siller, G.; Lehtinen, O.; Wang, F. C.; Nair, R. R.; Kaiser, U.; Wu, H. A.; Geim, A. K.; Grigorieva, I. V. Square Ice in Graphene Nanocapillaries. *Nature* **2015**, *519*, 443–445.
- (30) Amadei, C. A.; Vecitis, C. D. How to Increase the Signal-to-Noise Ratio of Graphene Oxide Membrane Research. *J. Phys. Chem. Lett.* **2016**, *7*, 3791–3797.
- (31) Talyzin, A. V.; Hausmaninger, T.; You, S.; Szabó, T. The Structure of Graphene Oxide Membranes in Liquid Water, Ethanol and Water-Ethanol Mixtures. *Nanoscale* **2014**, *6*, 272–281.
- (32) Xia, S.; Ni, M.; Zhu, T.; Zhao, Y.; Li, N. Ultrathin graphene oxide nanosheet membranes with various d-spacing assembled using the pressure-assisted filtration method for removing natural organic matter. *Desalination* **2015**, *371*, 78–87.
- (33) Akbari, A.; Sheath, P.; Martin, S. T.; Shinde, D. B.; Shaibani, M.; Banerjee, P. C.; Tkacz, R.; Bhattacharyya, D.; Majumder, M. Large-Area Graphene-Based Nanofiltration Membranes by Shear Alignment of Discotic Nematic Liquid Crystals of Graphene Oxide. *Nat. Commun.* **2016**, *7*, 10891.
- (34) Michl, J.; Thulstrup, E. Spectroscopy with Polarized Light: Solute Alignment by Photoselection. *Liquid Crystals, Polymers and Membranes*; VCH: New York, 1986.
- (35) Cole, K. C.; Aiji, A. In *Solid Phase Processing of Polymers*; Ward, I. M., Coates, P. D., Dumoulin, M. M., Eds.; Hanser Publishers: Munich, 2000; pp 33–84.
- (36) Zannoni, C. In *The Molecular Physics of Liquid Crystals*; Luckhurst, G. R., Gray, G. W., Eds.; Academic Press, 1979; pp 51–83.
- (37) Schneider, D. J.; Freed, J. H. In *Biological Magnetic Resonance*; Berliner, L. J., Ed.; Plenum Press: New York, 1989; pp 1–6.
- (38) Freed, J. H. In *Spin Labeling: Theory and Applications*; Berliner, L. J., Ed.; Plenum Press: New York, 1976; pp 53.
- (39) Budil, D. E.; Lee, S.; Saxena, S.; Freed, J. H. Nonlinear-Least-Squares Analysis of Slow-Motion EPR Spectra in One and Two Dimensions Using a Modified Levenberg–Marquardt Algorithm. *J. Magn. Reson., Ser. A* **1996**, *120*, 155–189.
- (40) Barnes, J. P.; Freed, J. H. Dynamics and Ordering in Mixed Model Membranes of Dimyristoylphosphatidylcholine and Dimyristoylphosphatidylserine: A 250-GHz Electron Spin Resonance Study Using Cholestane. *Biophys. J.* **1998**, *75*, 2532–2546.
- (41) Cassol, R.; Ge, M.-T.; Ferrarini, A.; Freed, J. H. Chain Dynamics and the Simulation of Electron Spin Resonance Spectra from Oriented Phospholipid Membranes. *J. Phys. Chem. B* **1997**, *101*, 8782–8789.
- (42) Vorobiev, A. K.; Chumakova, N. A. In *Nitroxides Theory, Experiment and Applications*; Kokorin, A. J., Ed.; INTECH: Rijeka, 2012; pp 57–112.
- (43) Vorobiev, A. K.; Yankova, T. S.; Chumakova, N. A. Orientation Distribution Function and Order Parameters of Oriented Spin Probe as Determined by EPR Spectroscopy. *Chem. Phys.* **2012**, *409*, 61–73.
- (44) Chumakova, N. A.; Yankova, T. S.; Fairfull-Smith, K. E.; Bottle, S. E.; Vorobiev, A. K. Molecular Orientational Order of Nitroxide Radicals in Liquid Crystalline Media. *J. Phys. Chem. B* **2014**, *118*, 5589–5599.
- (45) Danilenko, A. M.; Boguslavsky, E. G.; Nadolinny, V. A.; Gromilov, S. A.; Grigor'ev, I. A.; Rejser, E. Intercalation Compounds of Fluorographite and Graphite Oxide with Spin Probes. *Appl. Magn. Reson.* **2003**, *24*, 225–232.
- (46) Pham, C. V.; Krueger, M.; Eck, M.; Weber, S.; Erdem, E. Comparative Electron Paramagnetic Resonance Investigation of Reduced Graphene Oxide and Carbon Nanotubes with Different Chemical Functionalities for Quantum Dot Attachment. *Appl. Phys. Lett.* **2014**, *104*, 132102.
- (47) Pham, C. V.; Repp, S.; Thomann, R.; Krueger, M.; Weber, S.; Erdem, E. Charge Transfer and Surface Defect Healing within ZnO Nanoparticle Decorated Graphene Hybrid Materials. *Nanoscale* **2016**, *8*, 9682–9687.
- (48) Szabó, T.; Berkesi, O.; Forgó, P.; Josepovits, K.; Sanakis, Y.; Petridis, D.; Dékány, I. Evolution of Surface Functional Groups in a

Series of Progressively Oxidized Graphite Oxides. *Chem. Mater.* **2006**, *18*, 2740–2749.

(49) Ćirić, L. C.; Sienkiewicz, A.; Djokic, D. M.; Smajda, R.; Magrez, A.; Kaspar, T.; Nesper, R.; Forro, L. Size Dependence of the Magnetic Response of Graphite Oxide and Graphene Flakes—an Electron Spin Resonance Study. *Phys. Status Solidi B* **2010**, *247*, 2958–2961.

(50) Sun, J.; Morales-Lara, F.; Klechikov, A.; Talyzin, A. V.; Baburin, I. A.; Seifert, G.; Cardano, F.; Baldrighi, M.; Frascioni, M.; Giordani, S. Porous Graphite Oxide Pillared with Tetrapod-Shaped Molecules. *Carbon* **2017**, *120*, 145–156.

(51) Zhidomirov, G. M., Lebedev, Ia. S., Dobriakov, C. A., Shtenshneider, N. Ia., Chirkov, A. K., Gubanov, V. A. *Interpretation of Complex EPR Spectra*; Nauka: Moscow, Russia, 1975.

(52) Dennis, J. E.; Gay, D. M.; Walsh, R. E. An Adaptive Nonlinear Least-Squares Algorithm. *ACM Trans. Math Software* **1981**, *7*, 348–368.

(53) Goldman, S. A.; Bruno, G. V.; Freed, J. H. Estimating Slow-Motional Rotational Correlation Times for Nitroxides by Electron Spin Resonance. *J. Phys. Chem.* **1972**, *76*, 1858–1860.

(54) Ottaviani, M. F.; Garcia-Garibay, M.; Turro, N. J. TEMPO radicals as EPR probes to monitor the adsorption of different species into X zeolite. *Colloids Surf., A* **1993**, *72*, 321–332.

(55) Marcano, D. C.; Kosynkin, D. V.; Berlin, J. M.; Sinitskii, A.; Sun, Z.; Slesarev, A.; Alemany, L. B.; Lu, W.; Tour, J. M. Improved Synthesis of Graphene Oxide. *ACS Nano* **2010**, *4*, 4806–4814.